

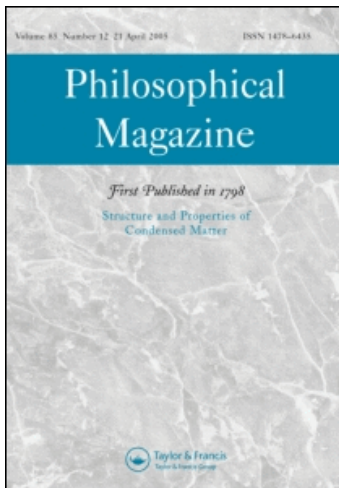
This article was downloaded by: [CAS Chinese Academy of Sciences]

On: 31 March 2010

Access details: Access Details: [subscription number 917035559]

Publisher Taylor & Francis

Informa Ltd Registered in England and Wales Registered Number: 1072954 Registered office: Mortimer House, 37-41 Mortimer Street, London W1T 3JH, UK



Philosophical Magazine

Publication details, including instructions for authors and subscription information:

<http://www.informaworld.com/smpp/title~content=t713695589>

Microstructural evolution of $[\text{PbZr}_{x-1}\text{Ti}_1-x\text{O}_3/\text{PbZr}_y\text{Ti}_{1-y}\text{O}_3]_n$ epitaxial multilayers ($x/y = 0.2/0.4, 0.4/0.6$)-dependence on layer thickness

Y. L. Zhu^a; S.J. Zheng^a; X. L. Ma^a; L. Feigl^b; M. Alexe^b; D. Hesse^b; I. Vrejoiu^b

^a Shenyang National Laboratory for Materials Science, Institute of Metal Research, Chinese Academy of Sciences, Shenyang 110016, P.R. China ^b Max Planck Institute of Microstructure Physics, Weinberg 2, D-06120 Halle, Germany

Online publication date: 30 March 2010

To cite this Article Zhu, Y. L. , Zheng, S.J. , Ma, X. L. , Feigl, L. , Alexe, M. , Hesse, D. and Vrejoiu, I.(2010) 'Microstructural evolution of $[\text{PbZr}_{x-1}\text{Ti}_1-x\text{O}_3/\text{PbZr}_y\text{Ti}_{1-y}\text{O}_3]_n$ epitaxial multilayers ($x/y = 0.2/0.4, 0.4/0.6$)-dependence on layer thickness', Philosophical Magazine, 90: 10, 1359 – 1372

To link to this Article: DOI: 10.1080/14786430903352656

URL: <http://dx.doi.org/10.1080/14786430903352656>

PLEASE SCROLL DOWN FOR ARTICLE

Full terms and conditions of use: <http://www.informaworld.com/terms-and-conditions-of-access.pdf>

This article may be used for research, teaching and private study purposes. Any substantial or systematic reproduction, re-distribution, re-selling, loan or sub-licensing, systematic supply or distribution in any form to anyone is expressly forbidden.

The publisher does not give any warranty express or implied or make any representation that the contents will be complete or accurate or up to date. The accuracy of any instructions, formulae and drug doses should be independently verified with primary sources. The publisher shall not be liable for any loss, actions, claims, proceedings, demand or costs or damages whatsoever or howsoever caused arising directly or indirectly in connection with or arising out of the use of this material.

Microstructural evolution of $[\text{PbZr}_x\text{Ti}_{1-x}\text{O}_3/\text{PbZr}_y\text{Ti}_{1-y}\text{O}_3]_n$ epitaxial multilayers ($x/y=0.2/0.4, 0.4/0.6$) – dependence on layer thickness

Y.L. Zhu^{a*}, S.J. Zheng^a, X.L. Ma^a, L. Feigl^b, M. Alexe^b, D. Hesse^b and I. Vrejoiu^b

^aShenyang National Laboratory for Materials Science, Institute of Metal Research, Chinese Academy of Sciences, Shenyang 110016, P.R. China; ^bMax Planck Institute of Microstructure Physics, Weinberg 2, D-06120 Halle, Germany

(Received 20 July 2009; final version received 21 September 2009)

The microstructure of ferroelectric $[\text{PbZr}_x\text{Ti}_{1-x}\text{O}_3/\text{PbZr}_y\text{Ti}_{1-y}\text{O}_3]_n$ epitaxial multilayers ($x/y=0.2/0.4, 0.4/0.6$) deposited on SrRuO_3 -coated SrTiO_3 substrates by pulsed-laser deposition with different layer periodicity and layer thickness was characterized by means of transmission electron microscopy. Electron diffraction and contrast analysis revealed a very clear and well-separated layer sequence. The microstructures of $\text{PbZr}_{0.2}\text{Ti}_{0.8}\text{O}_3/\text{PbZr}_{0.4}\text{Ti}_{0.6}\text{O}_3$ and $\text{PbZr}_{0.4}\text{Ti}_{0.6}\text{O}_3/\text{PbZr}_{0.6}\text{Ti}_{0.4}\text{O}_3$ multilayers show a similar tendency in the dependence on the individual layer thickness. Whereas with thick individual layers, tetragonal a -domains are confined to specific layers of the two types of multilayers, below a certain critical thickness of the individual layers, a -domains extend over the whole film. This indicates a transition into a uniform tetragonal lattice and strain state of the whole multilayer. Increasing the layer periodicity further, the interfaces in $\text{PbZr}_{0.4}\text{Ti}_{0.6}\text{O}_3/\text{PbZr}_{0.6}\text{Ti}_{0.4}\text{O}_3$ multilayers become rough, and complex a -domain configurations appear.

Keywords: ferroelectrics; transmission electron microscopy; microstructure

1. Introduction

Ferroelectric oxides have received much attention because of their promising application potential in many fields, including sensors, actuators, high-density non-volatile memories, and other storage media [1–12]. Traditionally, most of these efforts have dealt with single-phase thin films, but an important technique that has emerged recently involves heterolayered thin films or superlattices consisting of alternate layers of materials, phases and structures as well as compositional gradient structures. Recent studies have shown that oxide multilayers or superlattices, such as $\text{BaTiO}_3/\text{SrTiO}_3$, $\text{PbZr}_{0.4}\text{Ti}_{0.6}\text{O}_3/\text{PbZr}_{0.6}\text{Ti}_{0.4}\text{O}_3$, $\text{PbZrO}_3/\text{PbZr}_{0.8}\text{Ti}_{0.2}\text{O}_3$ or $\text{PbZr}_{0.4}\text{Ti}_{0.6}\text{O}_3/\text{PbZrO}_3$, provide quite different properties compared with single thin films of each of these oxides [13–17]. In other words, adjusting

*Corresponding author. Email: ylzhu@imr.ac.cn

the composition/periodicity in these multilayers allows for an additional degree of freedom and thus results in the possibility to tune the final properties.

Domain formation in ferroelectric compounds with tetragonal perovskite structure has been a hot topic both experimentally [8,18] and theoretically [19,20] due to its crucial role in ferroelectric device performance. It is known that domain formation is a result of transformation strain release during the paraelectric to ferroelectric transition [18]. Three types of domain were identified including *c*-domains, in which the *c*-axis of a tetragonal ferroelectric is normal to the film/substrate interface, *a*₁-domains, in which an *a*-axis of the ferroelectric is normal to the film/substrate interface with the tetragonal *c*-axis and the other *a*-axis in the plane of the interface, and *a*₂-domains, which are rotated by 90° about the surface normal relative to the *a*₁-domains. Control of domain structures is essential, because the properties of ferroelectric films strongly depend on the relative volume fraction, spatial distribution, and mobility of domain walls. It was reported that PbZr_{0.35}Ti_{0.65}O₃ films with a rather low volume fraction of *c*-domains of 0.2–0.4 show enhanced ferroelectric and piezoelectric properties by *a*-to-*c* domain switching [5,21]. The mobility of 90° domains in PbZr_{0.2}Ti_{0.8}O₃ films under non-uniform electric field results in enhanced capacitance and improved piezoelectric properties [22]. The morphology of 90° domains in bilayers and superlattices can vary under different conditions and result in drastic changes of the electrical properties [23].

Generally, interfacial structure and microstructure in thin films are of interest because of their potential influence on the electrical properties. Notwithstanding the extensive physical property investigations on ferroelectric multilayers and superlattices [13–17,21], a detailed and comprehensive understanding from the microstructural point of view has not been achieved so far. In this paper, the characterization by transmission electron microscopy (TEM) is reported of PbZr_{*x*}Ti_{1-*x*}O₃/PbZr_{*y*}Ti_{1-*y*}O₃ epitaxial multilayers (*x*/*y* = 0.2/0.4, 0.4/0.6) with different layer periodicities and layer thicknesses, grown on vicinal (100) SrTiO₃ substrates with SrRuO₃ bottom electrodes. The investigation revealed a clear dependence of the microstructure of these two types of multilayers on the thickness of the individual layers.

2. Experimental

[PbZr_{*x*}Ti_{1-*x*}O₃/PbZr_{*y*}Ti_{1-*y*}O₃]_{*n*} epitaxial multilayers (*x*/*y* = 0.2/0.4, 0.4/0.6; *n* = 2, 4, 11, 20, 21, 30 and 60), where *n* represents the number of stacked sublayers, were prepared by pulsed-laser deposition (PLD). All multilayers were grown at a substrate temperature of 575°C in 0.3 mbar oxygen pressure. Vicinal single crystalline SrTiO₃ (STO)(100) substrates with a miscut angle of about 0.1° were used (cf. [24]). Single crystalline SrRuO₃ (SRO) layers, grown in step-flow growth mode, served as bottom electrodes. Multilayers consisting of PbZr_{0.2}Ti_{0.8}O₃ (PZT20/80) and PbZr_{0.4}Ti_{0.6}O₃ (PZT40/60) sublayers were grown with *n* = 2, 11 and 21. Both top and bottom layers were PZT20/80 layers to assure a symmetric structure. The latter have a small lattice misfit with the substrate, which is helpful to achieve a layer-by-layer growth. Multilayers consisting of PbZr_{0.4}Ti_{0.6}O₃ (PZT40/60) and PbZr_{0.6}Ti_{0.4}O₃ (PZT60/40) sublayers were grown with *n* = 4, 20, 30 and 60. In this case, top and bottom layers

were of different composition. The thickness of the individual layers was in the range 2–30 nm. Detailed deposition procedures can be found elsewhere [15,25].

Thin foils for cross-sectional TEM observation were prepared by the conventional method, i.e. by slicing, grinding, dimpling, and finally ion-milling. A Philips CM20T electron microscope was used at the very beginning of this work. A Tecnai F30 transmission electron microscope with a point resolution of 0.17 nm and working at 300 kV was used to carry out high-resolution lattice imaging.

3. Results and discussion

[PZT20/80/PZT40/60] bi- and multilayers were prepared by stacking a PZT20/80 and a PZT40/60 layer on SRO/STO. The crystal structure of both compositions is tetragonal, and both are ferroelectric at room temperature [26]. Figure 1 shows a bright-field image of such a [PZT20/80/PZT40/60]₂ bilayer (sample 1) and also the corresponding electron diffraction pattern taken from the area including the films and the SRO/STO substrate. The first layer grown on SRO/STO is PZT 20/80, which exhibits a sharp and flat interface with the substrate, followed by the PZT40/60 layer, in which contrast variations can be observed. Each layer is about 30 nm in thickness.

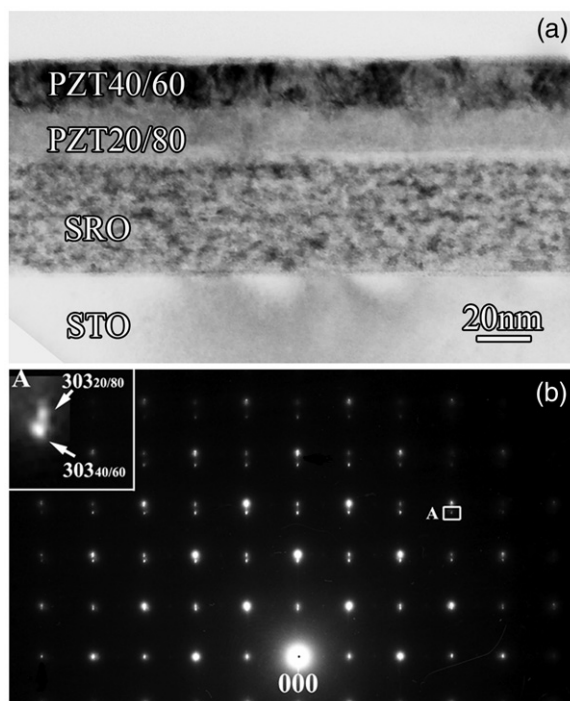


Figure 1. Bright-field image of a [PZT20/80/PZT40/60]₂ bilayer and the corresponding electron diffraction pattern taken from the area including the films and SRO/STO substrate. The inset displays the spot splitting caused by different lattice parameters of PZT20/80 and PZT40/60.

Because the room temperature in-plane lattice parameter of PZT20/80 ($a_{\text{in-plane}} = 0.3935 \text{ nm}$) is quite close to that of STO ($a = 0.3905 \text{ nm}$), the lattice misfit between them is rather small ($\sim 0.7\%$). Therefore, the PZT20/80 layer may be coherently grown on the substrate and no obvious strain contrast caused by misfit dislocations can be observed along the interface. In comparison, PZT40/60 ($a_{\text{in-plane}} = 0.3985 \text{ nm}$) shows a relatively large lattice misfit with the substrate, and thus misfit dislocations may be found along the interface. Other lattice distortions may also form in the second layer and thus cause the strain contrast. The spot splitting in the electron diffraction pattern verifies the lattice parameter differences between the layers, as shown in Figure 1b. The outer spot stems from PZT20/80, whereas the inner one from PZT40/60.

Cross-sectional high-resolution transmission electron microscopy (HRTEM) confirmed the coherent growth of PZT20/80 on SRO/STO, as shown in Figure 2. Horizontal pairs of arrows denote the positions of interfaces. As expected, misfit dislocations could not be observed along the interface between the bottom PZT20/80 and SRO/STO, whereas they are visible along the interface between PZT20/80 and PZT40/60 layers.

A cross-sectional TEM image of [PZT20/80 / PZT40/60]₁₁ (sample 2) is displayed in Figure 3. Figure 3a is a bright-field image, whereas Figure 3b is a dark-field image. The thickness of the individual layers is around 16 nm. Each layer is clearly discerned with obvious interfaces between them. The remarkable feature in this micrograph is that ferroelectric 90° a - c domains appear and show a rather complex configuration. Some of them extend over several layers, or even over the entire film, while many others are confined to specific single layers. As can be seen from Figure 4, taken from the bottom area near the interface between the film and the substrate along the [010] direction of STO, a -domains are found only in PZT20/80 layers, as indicated by white arrows. These a -domains are rather narrow with a width of around 2 nm or

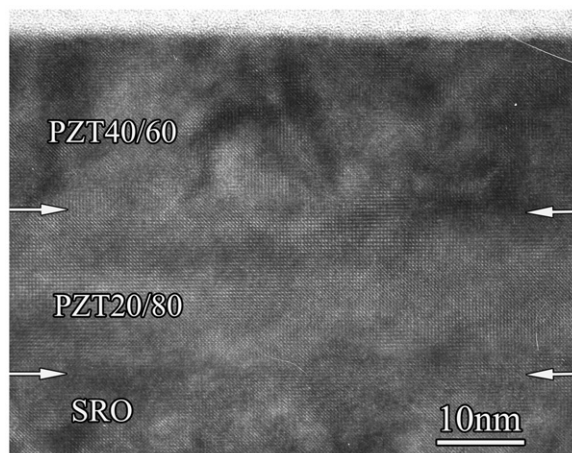


Figure 2. Cross-sectional HRTEM image of a PZT20/80 / PZT40/60 bilayer taken along [010] STO. The first PZT20/80 layer is coherently grown on SRO/STO. Misfit dislocations can be observed along the interface between PZT20/80 and PZT40/60.

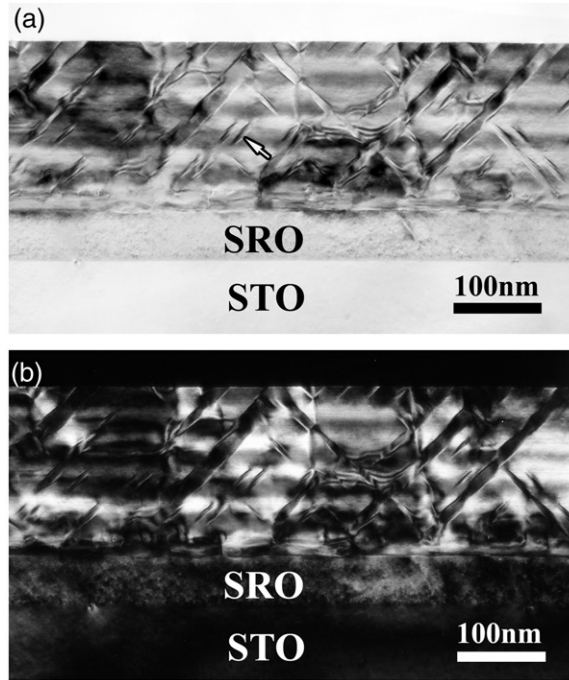


Figure 3. Cross-sectional TEM image of a $[\text{PZT}_{20/80}/\text{PZT}_{40/60}]_{11}$ structure. Some a -domains confined to individual layers can be observed. (a) Bright-field image; (b) dark-field image. The arrow in (a) points to an a -domain confined to a single layer.

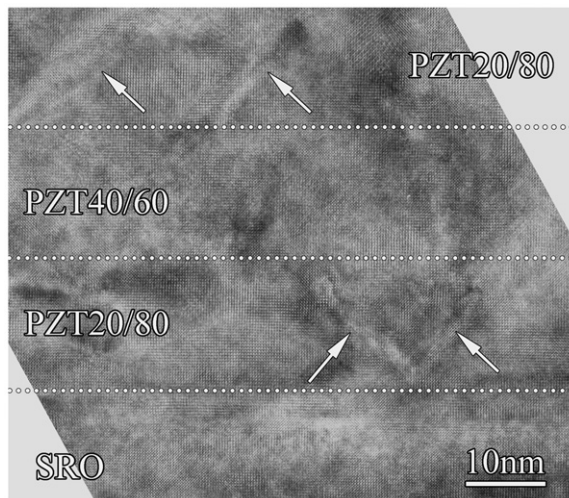


Figure 4. HRTEM image of a $[\text{PZT}_{20/80}/\text{PZT}_{40/60}]_{11}$ structure taken from the bottom area near the interface between the film and the substrate along the $[010]$ direction of STO. The confined a -domains are found only in PZT20/80 layers as indicated by white arrows.

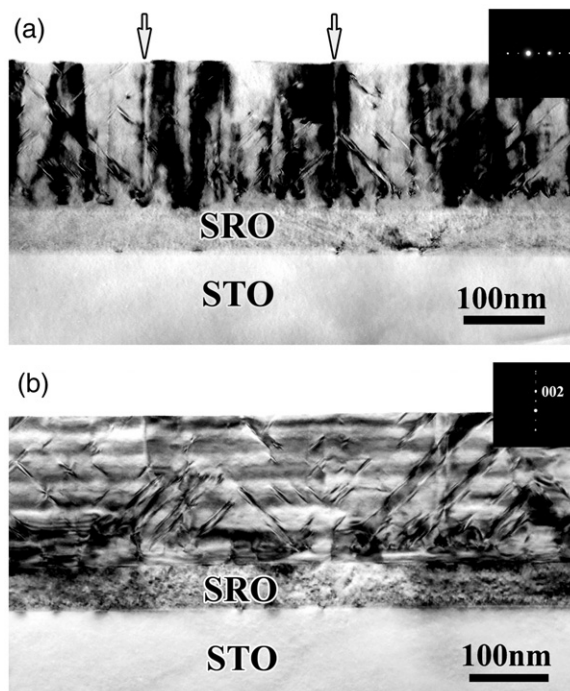


Figure 5. Cross-sectional bright-field TEM images of a $[\text{PZT}_{20}/80/\text{PZT}_{40}/60]_{11}$ structure taken under different two-beam conditions: (a) $\mathbf{g} = 020$; (b) $\mathbf{g} = 002$. Vertical arrows point to two threading dislocations in (a).

less, implying the initial formation of a -domains in the PZT20/80 layers. The bottom layer of PZT20/80 shows a distinct and coherent interface with SRO. Besides a -domains, threading dislocations (TDs) are another major defect in the films.

Figure 5 shows cross-sectional bright-field TEM images of sample 2 taken under different two-beam conditions. In Figure 5a, which was taken with $\mathbf{g} = (020)$, threading dislocations are visible along the direction normal to the interface, whereas in Figure 5b, which was taken under $\mathbf{g} = (002)$, the TDs are out of contrast. According to the $\mathbf{g} \cdot \mathbf{b}$ extinction criterion, it can be concluded that the TDs have Burgers vectors parallel to the film/substrate interface and are pure edge dislocations.

To further elucidate the relationships between 90° ferroelectric domains and threading dislocations in sample 2, HRTEM imaging was carried out. Figure 6 shows a cross-sectional HRTEM image of a near-surface area showing the presence of threading dislocations together with a -domains. Vertical double arrows designate the threading dislocations in the micrograph, whereas horizontal pairs of white arrows denote the positions of interfaces between each layer. Oblique white arrows point out the a -domains. Here, the threading dislocations are dissociated into dipoles spanning a width of about 15–20 nm. It can also be noticed that these threading dislocation dipoles penetrate through the whole multilayer even crossing the a -domains, implying that the threading dislocation dipoles are already formed at

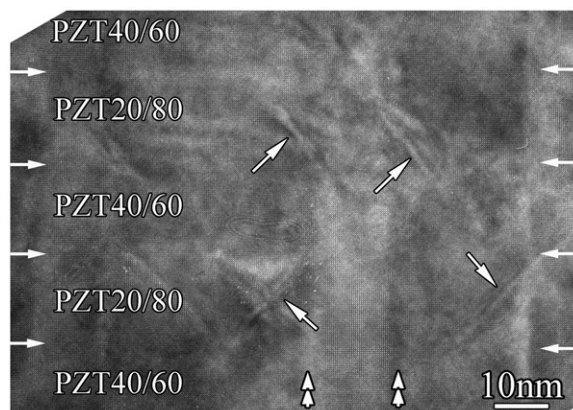


Figure 6. Cross-sectional HRTEM image of the surface-near area of a $[\text{PZT20/80}/\text{PZT40/60}]_{11}$ structure showing the presence of threading dislocations and a -domains. The two vertical double arrows designate a threading dislocation dipole. Pairs of horizontal white arrows denote the positions of interfaces between each layer. Oblique white arrows point out the a -domains.

growth temperature, or at least at a temperature higher than the ferroelectric phase transition temperature. In comparison, it is well known that ferroelectric domains are the product of the ferroelectric phase transformation during the cooling process. Similar observations were reported in PZT20/80 thin films grown on SRO/STO [27]. It was suggested that these threading dislocations may affect the ferroelectric properties of this kind of film through pinning the 180° ferroelectric domains.

Figure 7a shows a cross-sectional TEM image of a $[\text{PZT20/80}/\text{PZT40/60}]_{21}$ heterostructure with 21 layers (sample 3) and thinner individual PZT layers. The thickness of each individual layer is about 6 nm. From this image, it is evident that nearly all a -domains extend over the whole thickness and are not terminated at the interfaces. The typical width of the a -domains is around 10 nm. The electron diffraction pattern reveals the epitaxial growth of the multilayers, as shown in Figure 7b. Moreover, in addition to the strong diffraction spots from the film and the substrate, satellite spots along the interface normal can be observed in the magnified inset A. So the stacking periodicity of the superlattice can be calculated from the spacings of these superlattice spots in inset A. Inset B shows the spot splitting resulting from a and c domains as well as from the substrate. Because sample 1 has only two layers and the individual layers are thicker compared to those of samples 2 and 3, spot splitting between diffraction spots of PZT20/80 and PZT40/60 along the c^* -direction is relatively easy to be seen.

Cross-sectional HRTEM imaging of sample 3 indicates that typical 90° a - c ferroelectric domains usually stem from the interface between the first PZT20/80 and PZT40/60 layer, as shown in Figure 8. This image is a lattice image taken from the bottom area near the interface between the film and the substrate along $[010]$ direction of STO. The dotted line marks the interface between SRO and the first PZT20/80 layer. The interface is atomically smooth and no misfit dislocation can be observed along it, indicating the coherent growth of PZT20/80 on SRO/STO.

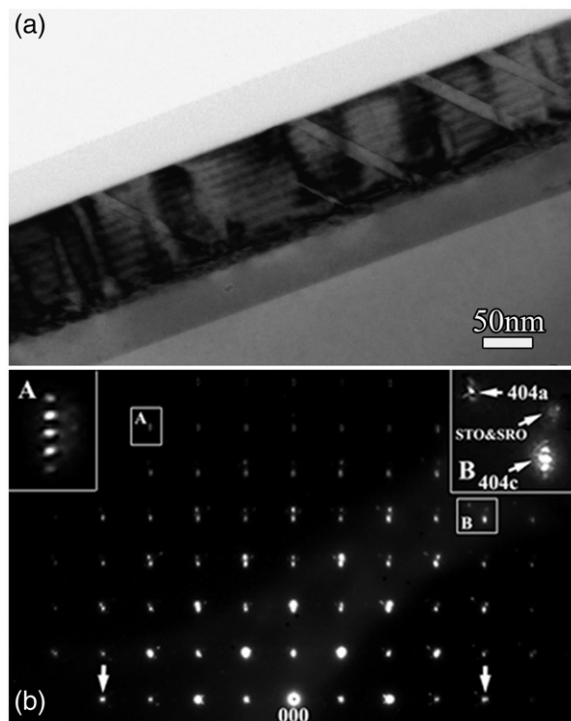


Figure 7. (a) Cross-sectional TEM image of a $[\text{PZT}_{20/80}/\text{PZT}_{40/60}]_{21}$ structure with very thin individual layers. It can be observed that nearly all a -domains extend over the whole thickness. (b) The corresponding electron diffraction pattern.

The absence of 90° boundaries in this first layer may be a consequence of the coherently strained state of this layer. Misfit dislocations can be identified along the interface between the bottom PZT_{20/80} layer and the next PZT_{40/60} layer, as denoted by a vertical arrow. Their presence is certainly due to the relatively large lattice misfit between these layers. The polar a - and c -directions are also given in the image. The tilting of the lattice of the twinned region (the c -domain) compared to the lattice of the a -domain was verified by a Fourier power spectrum of this image (inset). The misalignment between adjacent a - and c -domains was determined to be about 2.3° . However, besides the strong spots from a - and c -domains, spot splitting caused by the different lattice parameters of alternating PZT_{20/80} and PZT_{40/60} layers cannot be identified, implying a common strain state of the imaged area.

In contrast, a - and c -domains in the top area near the surface show larger misalignment and the corresponding angle there is about 3° , as measured from the HRTEM image of Figure 9. This image was taken from the area near the top surface. The interfaces between successive layers are atomically flat. Neither misfit dislocations nor strong lattice distortions along the interfaces can be observed; rather they are coherent interfaces. Similarly, separate spots for PZT_{20/80} and PZT_{40/60} due to their respective different lattice parameters were not found in the inset, indicating a uniform strain state in this image. The relatively large tilting angle

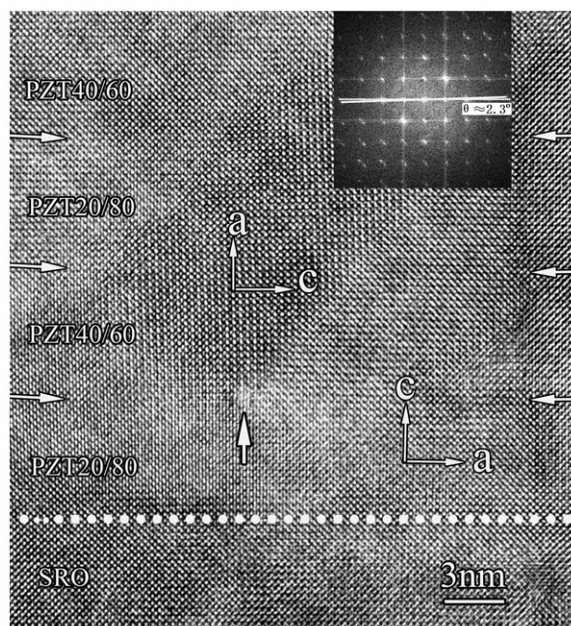


Figure 8. A lattice image of a $[\text{PZT20/80/PZT40/60}]_{21}$ structure taken from the bottom area near the interface between the film and the substrate along the $[010]$ direction of STO. The misalignment between adjacent a - and c -domains is reflected by the Fourier spectrum of the image (inset); the angle is about 2.3° .

implies that the lattice parameters of the top area of the superlattices are different from those of the bottom area of the films, which may be caused by different strain relaxation states in these two regions.

The microstructural evolution in $[\text{PZT20/80/PZT40/60}]$ multilayers with different individual layer sequence and thickness was discussed above based on TEM analysis. For comparison, $[\text{PZT60/40/PZT40/60}]$ multilayers with various individual layer sequence and thickness were also prepared by PLD and investigated by TEM. This kind of multilayer consists of rhombohedral PZT60/40 and tetragonal PZT40/60 [15], and the overall composition $(x+y)/2$ equals, or is close to, 0.5, which approaches the composition of the so-called morphotropic phase boundary of PZT52/48. It was reported that around this composition, PZT compounds reveal enhanced dielectric, ferroelectric and piezoelectric properties [14,28]. Similar microstructural variations were found in these multilayers. Figure 10a shows a cross-sectional TEM image of a four-layer structure, in which 90° a - c domains are only observable in some specific layers, i.e. in the PZT40/60 layers, demonstrating that each layer retains its rhombohedral and tetragonal structure, respectively. Each layer is about 30 nm thick. The interfaces are distinct. However, on increasing the number of layers while reducing the thickness of the individual layers, the situation becomes different, as shown in Figures 10b and c. Figure 10b reveals the overview of a 30-layer multilayer with each layer 3 nm thick, in which uniformly 90° a - c domains exist and extend over the whole film, indicating that the nominally rhombohedral

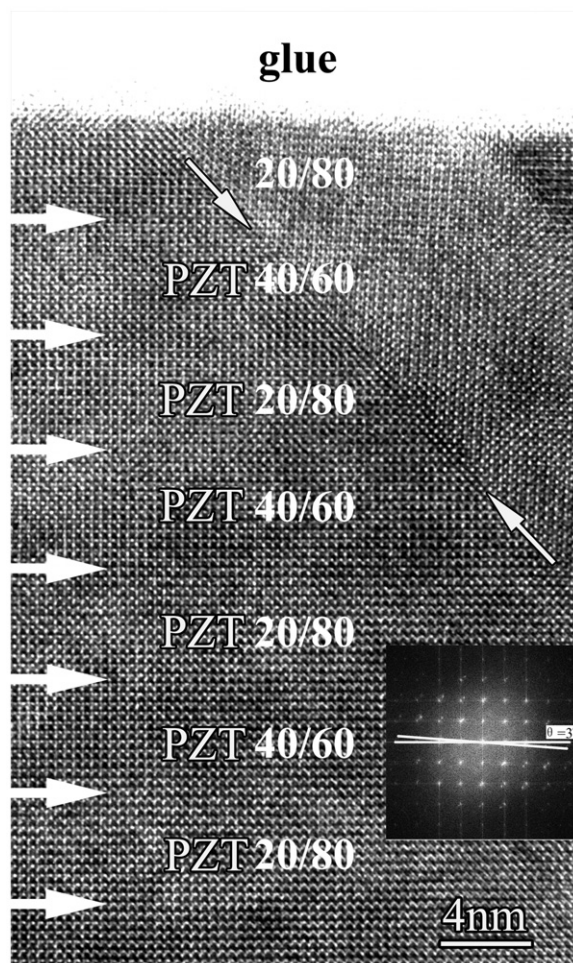


Figure 9. A lattice image of a $[\text{PZT}_{20/80}/\text{PZT}_{40/60}]_{21}$ structure taken from the area near the top surface. Interfaces between successive layers are atomically flat. The misalignment angle is about 3° , as can be seen in the Fourier spectrum of the image (inset).

PZT_{60/40} layers adopt a tetragonal structure, just like the case in our previous report [15]. Obviously, the compressive epitaxial strain imposed by the cubic substrate and possibly the interfacial strains inside the multilayers stabilize a tetragonal structure. Further increasing the number of layers, the interfaces in the multilayers deteriorate and get rough, as shown in Figure 10c. This multilayer consists of 60 layers, with a thickness of each layer of 2 nm only. From this micrograph, it is evident that the configuration of 90° a - c domains is now complex again, the domain boundaries being discontinuous. In this series of multilayers, misfit dislocations along the interface between the first deposited PZT_{40/60} layer and the SRO/STO substrate are found periodically distributed, as is visible from the strain contrasts in Figure 10.

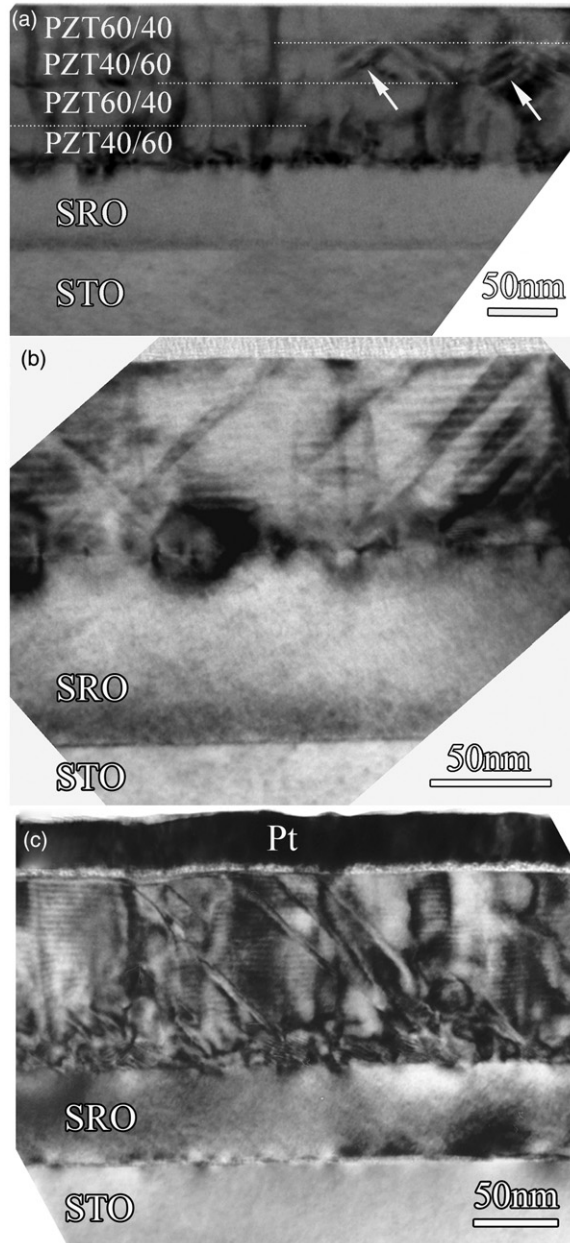


Figure 10. Bright-field images of $[\text{PZT60/40} / \text{PZT40/60}]_n$ multilayers. The number of layers is (a) $n=4$, (b) $n=30$ and (c) $n=60$, respectively. The arrows in (a) denote domains confined to a single layer of PZT40/60.

The present study clearly demonstrates that ferroelectric *a*-domain formation and distribution in $[\text{PbZr}_x\text{Ti}_{1-x}\text{O}_3/\text{PbZr}_y\text{Ti}_{1-y}\text{O}_3]_n$ epitaxial multilayers ($x/y = 0.2/0.4, 0.4/0.6$) are strongly correlated with the thickness of the individual layers as well as with layer sequence. This appears to confirm the important role of both size-effect and interfaces on microstructural characteristics. As first suggested by Roitburd [29], the formation of *a*- and *c*-domains is a means of strain relaxation in heteroepitaxial ferroelectric and ferroelastic films. Later, Speck et al. [30] developed a temperature-dependent domain stability map, incorporating the effects of lattice misfit, thermal expansion mismatch, cooling rate and depolarizing fields. It is well accepted that the formation of domain structure in ferroelectric films is strongly influenced by the mechanical strains arising from the lattice mismatch and/or difference of the thermal expansion coefficients between film and substrate.

In the present investigation, cross-sectional TEM observations showed that both types of $\text{PbZr}_x\text{Ti}_{1-x}\text{O}_3/\text{PbZr}_y\text{Ti}_{1-y}\text{O}_3$ epitaxial multilayers experience similar microstructural evolution with decreasing individual layer thickness and increasing layer stacking number: in samples with large thickness of the individual layers, *a*-domains are constrained to specific layers, whereas they extend over the entire film thickness in samples with very thin individual layers. Obviously, interfacial strains between the layers contribute much to this effect. In our previous report [25], the lattice parameter variations were measured from both X-ray diffraction reciprocal space mapping and electron diffraction in $\text{PbZr}_{0.2}\text{Ti}_{0.8}\text{O}_3/\text{PbZr}_{0.4}\text{Ti}_{0.6}\text{O}_3$ multilayers with 11 and 21 layers, the different strain relaxation states of the as-deposited multilayers were verified, and the different *a*-domain formation behavior as well as its influence on the physical properties were explained. It should be further pointed out that besides strain, interlayer coupling between each layer through internal elastic, electrical and electromechanical fields may also play an important role in domain selection and ferroelectric properties, as reported by Zhong et al. [11] and by Misirlioglu et al. [31].

For $\text{PbZr}_{0.6}\text{Ti}_{0.4}\text{O}_3/\text{PbZr}_{0.4}\text{Ti}_{0.6}\text{O}_3$ multilayers, a thin individual layer thickness and the epitaxial strain imposed by the single crystal STO substrate can even induce the rhombohedral PZT60/40 layers to adopt a tetragonal structure, as shown in Figures 10b and c. This again demonstrates the significant impact of size-effect and interfacial strain on domain formation and structural transition. A structural transition from orthorhombic to rhombohedral was also found in the PbZrO_3 layers within $\text{PbZrO}_3/\text{Pb}(\text{Zr}_{0.8}\text{Ti}_{0.2})\text{O}_3$ epitaxial multilayers, when those were thinner than 10 nm [16].

It can be concluded that a thickness-dependent and strain-related transition takes place in these two types of multilayers below a certain critical thickness of individual layers. As a consequence, multilayers with different individual layer thickness and stacking periodicity show different electrical properties, as shown in [15,25].

4. Conclusions

Ferroelectric $\text{PbZr}_x\text{Ti}_{1-x}\text{O}_3/\text{PbZr}_y\text{Ti}_{1-y}\text{O}_3$ epitaxial multilayers ($x/y = 0.2/0.4, 0.4/0.6$) with different layer sequence and layer thickness were deposited on SrRuO_3 -coated SrTiO_3 substrates by pulsed-laser deposition and investigated using

transmission electron microscopy. Conventional TEM and HRTEM imaging revealed a very clear and well-separated layer sequence. The salient feature in $\text{PbZr}_{0.2}\text{Ti}_{0.8}\text{O}_3/\text{PbZr}_{0.4}\text{Ti}_{0.6}\text{O}_3$ and $\text{PbZr}_{0.4}\text{Ti}_{0.6}\text{O}_3/\text{PbZr}_{0.6}\text{Ti}_{0.4}\text{O}_3$ multilayers is a uniform strain state of the entire multilayer below a certain critical thickness of the individual layers, namely, a -domains propagate over the entire film thickness. In contrast, with thick individual layers, a -domains are constrained to specific individual layers.

Acknowledgements

This work was supported by the National Basic Research Program of China (2009CB623705), the National Natural Science Foundation of China (No. 50871115), and the German Research Foundation (DFG) under programs FOR 404 and SFB 762.

References

- [1] J.F. Scott, *Science* 315 (2007) p.954.
- [2] D. Schlom, L.Q. Chen, C.B. Eom, K. Rabe, S. Streiffer and J. Triscone, *Annu. Rev. Mater. Res.* 37 (2007) p.589.
- [3] D. Woodward, J. Knudsen and I. Reaney, *Phys. Rev. B* 72 (2005) p.104110.
- [4] C.L. Jia, S.B. Mi, K. Urban, I. Vrejoiu, M. Alexe and D. Hesse, *Phys. Rev. Lett.* 102 (2009) p.117601.
- [5] Y.K. Kim, H. Morioka and H. Funakubo, *J. Appl. Phys.* 101 (2007) p.064112.
- [6] B.S. Kwak, A. Erbil, J.D. Budai, M.F. Chisholm and L.A. Boatner, *Phys. Rev. B* 49 (1994) p.14865.
- [7] I. Vrejoiu, M. Alexe, D. Hesse and U. Goesele, *Adv. Funct. Mater.* 18 (2008) p.3892.
- [8] H. Nakaki, Y.K. Kim, S. Yokoyama, R. Ikariyama, H. Funakubo, S.K. Streiffer, K. Nishida, K. Saito and A. Gruverman, *J. Appl. Phys.* 104 (2008) p.064121.
- [9] V. Nagarajan, C.L. Jia, H. Kohlstedt, R. Waser, I.B. Misirlioglu, S.P. Alpay and R. Ramesh, *Appl. Phys. Lett.* 86 (2005) p.192910.
- [10] E.K.W. Goo, R.K. Mishra and G. Thomas, *J. Appl. Phys.* 52 (1981) p.2940.
- [11] S. Zhong, S.P. Alpay, A.L. Roytburd and J.V. Mantese, *IEEE Trans. Ultrason. Ferroelectrics Freq. Contr.* 53 (2006) p.2349.
- [12] Z.H. Zhou, J.M. Xue, W.Z. Li, J. Wang, H. Zhu and J.M. Miao, *J. Appl. Phys.* 96 (2004) p.5706.
- [13] T. Zhao, Z.H. Chen, F. Chen, W.S. Shi, H.B. Lu and G.Z. Yang, *Phys. Rev. B* 60 (1999) p.1697.
- [14] F.M. Pontes, E. Longo, E.R. Leite and J.A. Varela, *Appl. Phys. Lett.* 84 (2004) p.5470.
- [15] I. Vrejoiu, Y.L. Zhu, G. Le Rhun, M.A. Schubert, D. Hesse and M. Alexe, *Appl. Phys. Lett.* 90 (2007) p.072909.
- [16] K. Boldyreva, L. Pintilie, A. Lotnyk, I.B. Misirlioglu, M. Alexe and D. Hesse, *Appl. Phys. Lett.* 91 (2007) p.122915.
- [17] D.H. Bao, R. Scholz, M. Alexe and D. Hesse, *J. Appl. Phys.* 101 (2007) p.054118.
- [18] H. Nakaki, Y.K. Kim, S. Yokoyama, R. Ikariyama, H. Funakubo, K. Nishida and K. Saito, *Appl. Phys. Lett.* 91 (2007) p.112904.
- [19] J.S. Speck and W. Pompe, *J. Appl. Phys.* 76 (1994) p.466.
- [20] S.P. Alpay and A. Roytburd, *J. Appl. Phys.* 83 (1998) p.4714.
- [21] Y.K. Kim, H. Morioka, R. Ueno, S. Yokoyama, K. Lee, S. Baik and H. Funakubo, *Appl. Phys. Lett.* 88 (2006) p.252904.

- [22] G. Le Rhun, I. Vrejoiu, L. Pintilie, D. Hesse, M. Alexe and U. Gösele, *Nanotechnology* 17 (2006) p.3154.
- [23] L. Feigl, I.B. Misirlioglu, I. Vrejoiu, M. Alexe and D. Hesse, *J. Appl. Phys.* 105 (2009) p.061607.
- [24] I. Vrejoiu, G. Le Rhun, L. Pintilie, D. Hesse, M. Alexe and U. Gösele, *Adv. Mater.* 18 (2006) p.1657.
- [25] L. Feigl, S.J. Zheng, B.I. Birajdar, B.J. Rodriguez, Y.L. Zhu, M. Alexe and D. Hesse, *J. Phys. Appl. Phys.* 42 (2009) p.085305.
- [26] E. Sawaguchi, *J. Phys. Soc. Jpn.* 8 (1953) p.615.
- [27] I. Vrejoiu, G. Le Rhun, N.D. Zakharov, D. Hesse, L. Pintilie and M. Alexe, *Phil. Mag.* 86 (2006) p.4477.
- [28] S. Yokohama, Y. Honda, H. Morioka, T. Oikawa, H. Funakubo, T. Iijima, H. Matsuda and K. Saito, *Appl. Phys. Lett.* 83 (2003) p.2408.
- [29] A.L. Roitburd, *Phys. Status Solidi (a)* 37 (1976) p.329.
- [30] J.S. Speck, A. Seifert and W. Pompe, *J. Appl. Phys.* 76 (1994) p.477.
- [31] I.B. Misirlioglu, M. Alexe, L. Pintilie and D. Hesse, *Appl. Phys. Lett.* 91 (2007) p.022911.